AGU PUBLICATIONS

JGR

Journal of Geophysical Research: Oceans

RESEARCH ARTICLE

10.1002/2014JC010191

The role of morphology and wave-current interaction at tidal inlets: An idealized modeling analysis

Maitane Olabarrieta[1,2], W. Rockwell Geyer[3], and Nirnimesh Kumar[4]

[1]Civil and Coastal Engineering Department, ESSIE, University of Florida, Gainesville, Florida, USA, [2]Environmental Hydraulics Institute, Universidad de Cantabria, Santander, Spain, [3]Applied Ocean Physics and Engineering, Woods Hole Oceanographic Institution, Woods Hole, Massachusetts, USA, [4]Scripps Institution of Oceanography, University of California, San Diego, La Jolla, California, USA

Key Points:
- Inlet morphology plays a main role on currents, waves, and their interaction
- Inlet hydrodynamics dependent on the relative jet and wave momentum fluxes
- Hydrodynamic changes result in different tracer transport patterns

Correspondence to:
M. Olabarrieta,
maitane.olabarrieta@essie.ufl.edu

Citation:
Olabarrieta, M., W. R. Geyer, and N. Kumar (2014), The role of morphology and wave-current interaction at tidal inlets: An idealized modeling analysis, *J. Geophys. Res. Oceans*, *119*, 8818–8837, doi:10.1002/2014JC010191.

Received 29 MAY 2014
Accepted 4 NOV 2014
Accepted article online 8 NOV 2014
Published online 23 DEC 2014

Abstract The outflowing currents from tidal inlets are influenced both by the morphology of the ebb-tide shoal and interaction with incident surface gravity waves. Likewise, the propagation and breaking of incident waves are affected by the morphology and the strength and structure of the outflowing current. The 3-D Coupled Ocean-Atmosphere-Wave-Sediment Transport (COAWST) modeling system is applied to numerically analyze the interaction between currents, waves, and bathymetry in idealized inlet configurations. The bathymetry is found to be a dominant controlling variable. In the absence of an ebb shoal and with weak wave forcing, a narrow outflow jet extends seaward with little lateral spreading. The presence of an ebb-tide shoal produces significant pressure gradients in the region of the outflow, resulting in enhanced lateral spreading of the jet. Incident waves cause lateral spreading and limit the seaward extent of the jet, due both to conversion of wave momentum flux and enhanced bottom friction. The interaction between the vorticity of the outflow jet and the wave stokes drift is also an important driving force for the lateral spreading of the plume. For weak outflows, the outflow jet is actually enhanced by strong waves when there is a channel across the bar, due to the "return current" effect. For both strong and weak outflows, waves increase the alongshore transport in both directions from the inlet due to the wave-induced setup over the ebb shoal. Wave breaking is more influenced by the topography of the ebb shoal than by wave-current interaction, although strong outflows show intensified breaking at the head of the main channel.

1. Introduction

Modification of flow hydrodynamics in tidal inlets and estuary mouths can play an important role for navigation, water quality monitoring, and prediction of morphologic changes [*Ozsoy and Unluata*, 1982]. Vertical structure of the velocity profile, spreading direction and rate, and velocity attenuation affect the transport and dispersion of the materials discharged by these effluents. Outflow velocity of jets decrease with distance from the inlet due to lateral momentum exchange, bed friction, and wave-current interaction. This flow deceleration leads to settling of suspended sediment, often resulting in the generation of a radial bar offshore of the inlet [*Hayes*, 1980; *Masselink and Hughes*, 2003]. The morphology of tidal inlets and the shape of the ebb shoal depend on the strength of the tidal outflow and on wave characteristics [*Hayes*, 1979; *Davis and Barnard*, 2003; *Nahon et al*., 2012].

Jet theory has been extensively used to predict ebb-tide flows from inlets in the absence of waves [e.g., *Bates*, 1953; *Borichansky and Mikhailov*, 1966; *Wright and Coleman*, 1974; *Ozsoy*, 1977; *Joshi*, 1982]. However, surface gravity wave effects have received relatively little attention, in spite of their potentially large influence on outflow dynamics. Experimental work performed by *Ismail* [1980] showed that in presence of opposing waves, momentum jets expand at a greater rate than in the absence of waves. Opposing waves also caused a decrease of the momentum density of the jet flow. In these laboratory experiments, the model basin was horizontal and the turbulent jet headed into opposing small amplitude surface waves. *Ismail and Wiegel* [1983] derived an analytical solution for the change of the spreading rate of momentum surface jets due to opposing surface gravity waves. Their theory predicted a linear increase in the rate of spreading of the jet due to impinging surface waves, scaled as the ratio of the wave momentum to the initial jet momentum density. *Nardin et al*. [2013], based on the work by *Joshi* [1982] and *Ismail and Wiegel*

[1983], developed an analytical model for the interaction between incoming waves and a turbulent expanding jet. This study was limited to a weak wave climate regime, with minimal wave breaking and absence of surf zone circulation. Also, these studies did not consider the role of an exterior bar and the possibility of depth-limited wave breaking.

Field observations of waves and currents in tidal inlets suggest a strong hydrodynamic influence of the ebb-tide shoal and wave-current interaction. Field measurements in Ponce de Leon inlet (Florida) [*Smith and Smith*, 2001] and Altamaha River Estuary (Georgia) [*Kang and Di Iorio*, 2006] showed that wave-current interaction in these specific inlets have smaller influence on the wave dynamics compared to the refraction, shoaling, and breaking produced by changing water depths over the ebb shoal. The ebb shoal has a dominant role in inducing depth-limited breaking and limiting the wave propagation and energy penetration to the inner part of the estuaries. *Olabarrieta et al*. [2011] applied the three-dimensional COAWST modeling system [*Warner et al*., 2010] with the vortex-force formalism in the Willapa inlet (Washington). During storm conditions the presence of the ebb shoal limited the amount of wave energy able to penetrate the inlet, resulting in a tidal modulation of the wave height in the inner part of the estuary. In these conditions, the depth-limited wave breaking-induced acceleration was the most important wave force and created changes in the jet flow direction and in the sea surface elevations both in the inlet and inside the estuary. *Dodet et al*. [2013] identified tidal induced wave modulations in the inlet area and a wave breaking-induced setup inside the Albufeira lagoon, Portugal. Although the ebb shoal in this inlet plays a primary role on the wave propagation, they observed that tidal current-induced changes on waves cannot be neglected since they substantially affect the seaward residual sediment transport. This paper demonstrated the relevance of considering the feedbacks between tidal currents and waves for an accurate morphodynamic prediction.

Field measurements and numerical models have also highlighted the relevance of wave-induced (surf zone) circulations in the ebb shoal area in energetic offshore wave conditions. *Robin et al*. [2009] analyzed the relative importance of different hydrodynamic processes on ebb delta bar migration in a macrotidal environment using detailed morphological and hydrodynamic measurements. Their study suggested that at this site, sediment transport and the modification in bar morphology were induced mainly by surf zone processes and associated littoral currents. During high surf conditions, mean flows were directed onshore with an absence of a bed return flow. *Bertin et al*. [2009] concluded that wave driven currents are responsible for the infilling of Obidos Inlet (Portugal) during storm conditions. *Delpey et al*. [2013] showed that wave-induced circulations can affect the water exchange between a small semienclosed estuary and the inner shelf. They found that wave breaking over a rocky shoal induced longshore currents that oppose and reduce the primary outflow of fresh water. Recent observations at the New River Inlet (North Carolina) showed that breaking-wave driven cross-shore radiation-stress gradients affect the along-inlet inlet mouth flows [*Wargula et al*., 2014].

Wave-current interaction and its effects have been more extensively studied within the surf zone, where breaking waves induce alongshore and rip currents [see *Haas et al*., 2003, and references therein]. The flow structure of rip currents is mostly similar to jet flows. These cellular circulations are often described as narrow, jet like, seaward directed flows. Rip currents are a particular kind of a jet flow since they are generated by wave forcing and this forcing is also affected by the rip current itself [e.g., *MacMahan et al*., 2006; *Weir et al*., 2011; *Bruneau et al*., 2011]. Therefore, the effects of wave-current interaction observed in this kind of hydrodynamic systems cannot be generalized for other types of jets.

This manuscript is aimed at quantifying the physical processes involved in the interaction between surface gravity waves and currents in inlets, including the consideration of ebb shoal morphology. The analysis is restricted to the interaction of a steady, planar, homopycnal jet subjected to weak and strong wave conditions. The flows can be representative of a river or stream discharge in a microtidal coast or of ebb currents in macro and mesotidal areas. The analysis is performed by considering two simplified inlet configurations characterized by the absence or presence of the most relevant morphologic elements observed in natural inlet systems: a well-developed central main channel and the exterior ebb shoal. For each inlet configuration a suite of three-dimensional, wave-current fully coupled numerical runs are performed. The effect of waves on the mean flow is incorporated by using the vortex force method [see *Uchiyama et al*., 2010; *Kumar et al*., 2012]. The results derived for each inlet configuration are compared to isolate the role of the inlet morphological elements (main channel and ebb shoal). In the analysis we also address the differences and similarities of wave-current interaction in previously analyzed rip current systems.

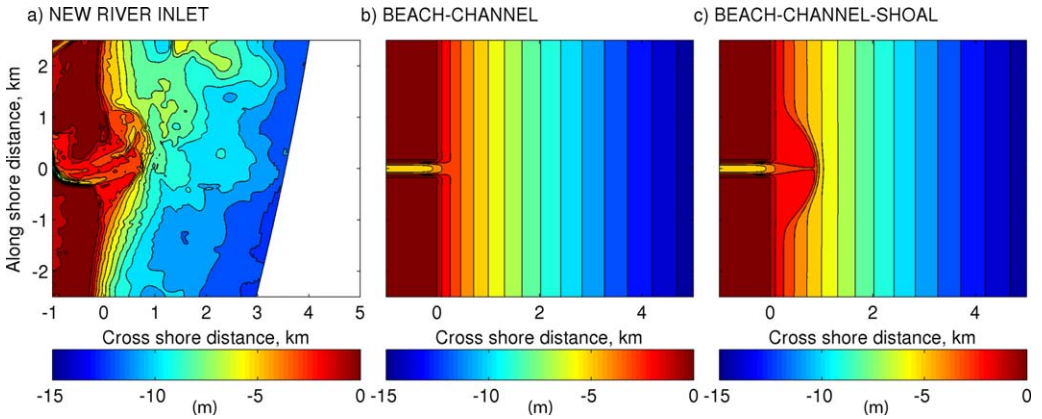

Figure 1. New River inlet bathymetry and considered idealized inlet configurations. (a) New River inlet morphology, 5 May 2012. (b) Idealized BEACH-CHANNEL configuration. (c) Idealized BEACH-CHANNEL-SHOAL configuration.

2. Methodology

In the present study, the Coupled Ocean-Atmosphere-Wave-Sediment Transport (COAWST) modeling system [*Warner et al*., 2010] has been applied. This modeling system couples the three-dimensional Regional Ocean Modeling System (ROMS) and the Simulating Waves Nearshore (SWAN) wind wave generation and propagation model.

ROMS is a three-dimensional, free surface, terrain-following numerical model that solves finite-difference approximations of the Reynolds-Averaged Navier-Stokes (RANS) equations using the hydrostatic and Boussinesq assumptions [*Chassignet et al*., 2000; *Haidvogel et al*., 2000] with a split-explicit time stepping algorithm [*Shchepetkin and McWilliams*, 2005; *Haidvogel et al*., 2008]. The wave-averaged momentum balance equations are based on the equations presented by *McWilliams et al*. [2004] and *Uchiyama et al*. [2010], which were implemented in the COAWST modeling system by *Kumar et al*. [2012]. For a detail description of the equations solved the reader is referred to *Olabarrieta et al*. [2011] and *Kumar et al*. [2012]. In these equations the effects of surface waves on the hydrodynamics are included by different conservative and nonconservative wave forces. The vortex force and the Bernoulli head are the conservative wave forces included in ROMS. The nonconservative wave forces considered in this study are the depth-induced wave breaking, whitecapping-induced flow accelerations, and the enhancement of the apparent bed roughness given by *Madsen* [1994].

Wave characteristics are computed with SWAN [*Booij et al*., 1999], a wave-averaged model that solves transport equations for wave action density. It accounts for shoaling and refraction, wind wave generation, wave breaking, bottom dissipation, and nonlinear wave-wave interactions. In the absence of momentum transfer from wind to wind waves, currents affect the wave propagation through the Doppler Effect and through the transport of the wave action by the absolute wave group celerity (sum of the relative group celerity and currents). Previous numerical modeling studies [*Ris and Holthuijsen*, 1996; *van der Westhuysen*, 2012; *Dodet et al*., 2013] and laboratory experiments [*Chawla and Kirby*, 2002] suggest steepening and subsequent breaking of waves in presence of strong opposing currents. Wave steepening due to currents is the result of the wavelength reduction due to opposing currents. This process is considered through the dispersion relation. *Booij et al*. [1999] presented a validation of current-induced shoaling and refraction using analytical expressions. When waves get too steep SWAN dissipates wave energy through the whitecapping dissipation process. In the default SWAN setting the whitecapping expression of *Komen et al*. [1984] is used. However, it is known that this expression underestimates wave dissipation in strong opposing currents, leading to an overestimation in the significant wave height [*Ris and Holthuijsen*, 1996].

SWAN can be run concurrently with the circulation model with a two-way coupling, whereby currents and sea surface elevations influence the wave field and waves affect the circulation. ROMS provides SWAN with the free surface elevations and currents within user specified time intervals. The currents are computed according to the formulation presented by *Kirby and Chen* [1989], which considers the vertical distribution of the current profile and the relative water depth of surface waves.

3. Model Setup and Analyzed Cases

The selected inlet configurations represent an idealized morphology with similar horizontal and vertical scales as New River inlet, North Carolina (Figure 1a). Like most of the inlets around the world, this inlet shows a high morphological variability in time and space as a response to external hydrodynamic forcing. The main channel and the ebb shoal change their orientation as well as their shape and volume. However, for the purpose of this study a simplified and static representation of the inlet morphology is considered.

Two idealized inlet configurations (shown in Figures 1b and 1c) are selected to analyze the role of these morphologic elements on the inlet hydrodynamics and the effects of wave-current interaction. The inlet mouth width and the channel depth are 300 and 5 m, respectively, in both cases. The first configuration (BEACH-CHANNEL) does not have any ebb shoal and it consists of a main channel that opens directly into a beach with a *Dean* [1977] profile, given by the expression $h = Ax^{2/3}$, where h is the depth of the profile with respect to the mean water level, A (=0.05) is a profile scale factor, and x is the distance offshore (in this case from the inlet mouth). The maximum water depth at the offshore boundary is 15 m (Figure 1b). The cross-shore and alongshore extensions of the study domain are 11 and 13 km, respectively. The second configuration (BEACH-CHANNEL-SHOAL) has a well-developed, symmetric ebb shoal, which extends 1 km offshore of the inlet mouth (Figure 1c). The minimum water depth at the ebb shoal is 2 m with respect to the still mean water level. The main channel, with a shallow bar close to the inlet mouth, crosses the whole ebb shoal connecting the inlet with the offshore area. This channel-bar-ebb shoal bathymetry is similar to the morphology observed in wave-dominated inlets with normal wave approach [see *Wright*, 1977; *Masselink and Hughes*, 2003].

The horizontal numerical grids used in ROMS and SWAN are defined with a Cartesian horizontal coordinate system, with a 30 m constant resolution. The ROMS grid vertically follows a sigma-coordinate system with 10 terrain-following equidistant grid cells. The boundary conditions are specified as follows: a Chapman boundary condition [*Chapman*, 1985] for the free surface elevation and a clamped condition for the 2-D and 3-D fluxes are imposed in the west (where the river outflow is defined). A Neumann boundary condition is imposed for the barotropic velocities and the free surface elevation in the northern, southern, and eastern boundaries. In the west the longitudinal component of the velocity is specified in a way that the outflow is set to 0, 325, 750, 1500, and 2250 m^3/s depending on the experiment. The temperature and salinity are considered constant and possible stratified flow conditions are not taken into account. The Coriolis parameter is set to zero in most of the experiments to isolate the effects of the morphology and wave-current interaction. However, the effect of this specific forcing (with a value corresponding to the latitude of New River inlet (NC), 34.5°N) is investigated later in the manuscript. Bed friction is computed assuming a bed roughness length corresponding to a grain size of 0.2 mm and a hydrodynamically rough flow. In most of the simulations the increase of the apparent bed roughness due to waves is not considered. However, the effect of the bottom roughness increase due to waves is described in section 5.1. The eddy viscosity value was set to 1.0 m^2/s. This value has been selected based on *Madsen et al*. [1988] but, as it is the case for the bed roughness, should be calibrated with measurements for nonidealized applications. In ROMS, a 20 s baroclinic (three-dimensional) time step is used with a mode-splitting ratio of 10 leading to a barotropic (two-dimensional) time stepping of 2 s.

In SWAN a constant single peak JONSWAP spectrum is defined along the eastern boundary. The wave directional spectrum is defined by 40 frequency (0.01–1 Hz) and 90 directional bands, restricting the wave propagation to the first and second quadrants. The depth induced breaking is modeled with the bore-based model of *Eldeberky and Battjes* [1996], with a breaking parameter γ of 0.73 (default value). Different wave conditions are analyzed varying the significant wave height (H_s) between 0 and 2 m, the peak period (T_p) from 5 to 10 s (typical sea and swell conditions in New River Inlet). All wave conditions correspond to normally incident waves with an angle of 90° (nautical convection). ROMS and SWAN exchanged data every 600 s. Different numerical runs with smaller exchange data were performed to verify that the interexchange every 600 s did not affect current and wave results. All numerical experiments are simulated for 24 h, guarantying a steady or a dynamically steady state condition.

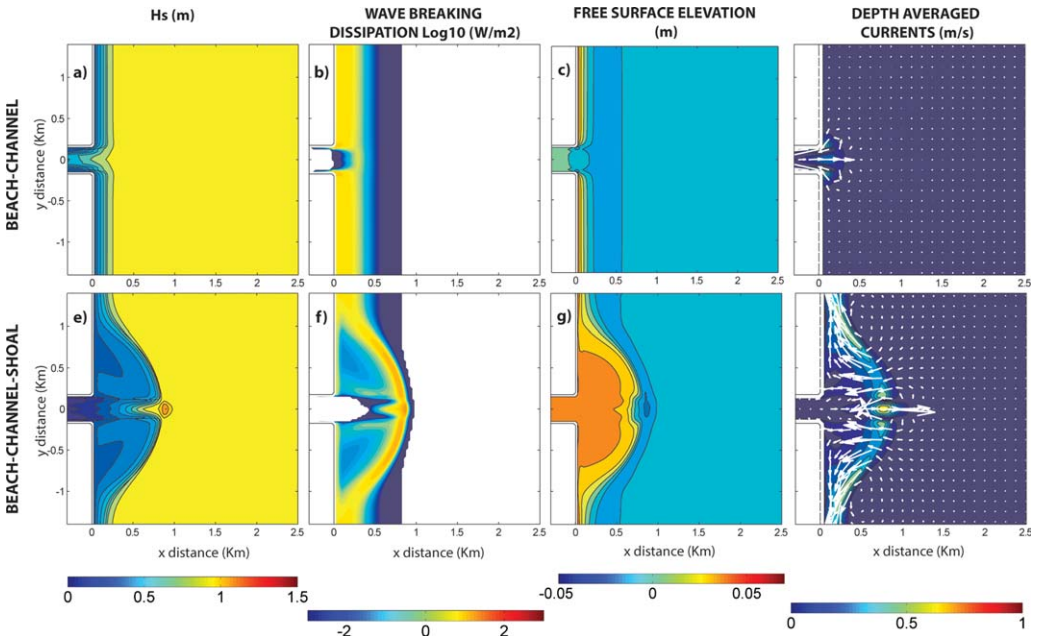

Figure 2. Morphology effect on wave propagation in the absence of outflow current. (top) The wave field characteristics in the CHANNEL-BEACH case: (a) significant wave height distribution, (b) logarithm of the wave dissipation, (c) wave-induced mean water elevation (m), and (d) barotropic Lagrangian currents. (bottom) The wave field characteristics in the BEACH-CHANNEL-SHOAL case: (e) significant wave height distribution, (f) logarithm of the wave dissipation, (g) wave-induced mean water elevation (m), and (h) barotropic Lagrangian currents. The waves at the offshore boundary are defined with a JONSWAP spectra ($H_s = 1.0$ m, $T_p = 7.5$ s, and normal incidence, representing a typical sea condition).

4. Results

4.1. Morphology Effect on Waves

The first set of numerical experiments considers only wave forcing with no outflow, which provides baseline cases to compare against the influence of the outflow jet.

In a simplified alongshore uniform beach, as waves propagate from the offshore toward the shore, decreasing water depths reduce the wavelength and the wave celerity. The process of wave shoaling increases the wave height until waves are depth limited, at which point they become unstable and break. The existence of an ebb shoal and the presence of a well-defined main channel produce significant changes in wave propagation due to refraction-diffraction processes. Surf zone circulations arising from alongshore variations of the wave breaking and oblique incidence in the breaking line also interact with the incoming wind waves and affect their propagation.

The spatial distributions of the significant wave height for the two inlet configurations, in the absence of forced inlet currents, are shown in Figures 2a and 2e. An offshore normally incident wave with 1.0 m offshore significant wave height, and 7.5 s peak period was considered. The associated depth averaged circulation in the inlet region is also presented (Lagrangian mean flows, defined as sum of Eulerian mean flow and Stokes drift; Figures 2d and 2h). The results depicted here include wave-current interaction, intended as the interaction between the waves and the water levels and currents they generate.

As expected, the horizontal distribution of the wave field is greatly dependent on the inlet configuration. In the absence of the ebb shoal, the alongshore variations of normally incident waves are localized in the inlet mouth. This alongshore variation in wave breaking produces an alongshore setup gradient (Figure 2c) that forces the water toward the channel and results on a localized return current (Figure 2d). The presence of the ebb shoal significantly modifies the wave propagation, causing ray bending and energy focusing toward the shallowest areas. For the most energetic wave conditions ($H_s \geq 1$ m), shallow water depths in the ebb shoal lead to depth limitation and wave breaking. Stokes drift and wave breaking-induced accelerations produce water mass transport from the shoal toward the shore (with current speeds up to 0.5 m/s when $H_s = 1.5$ m), creating a wave setup that increases near the inlet mouth. North and south of the ebb

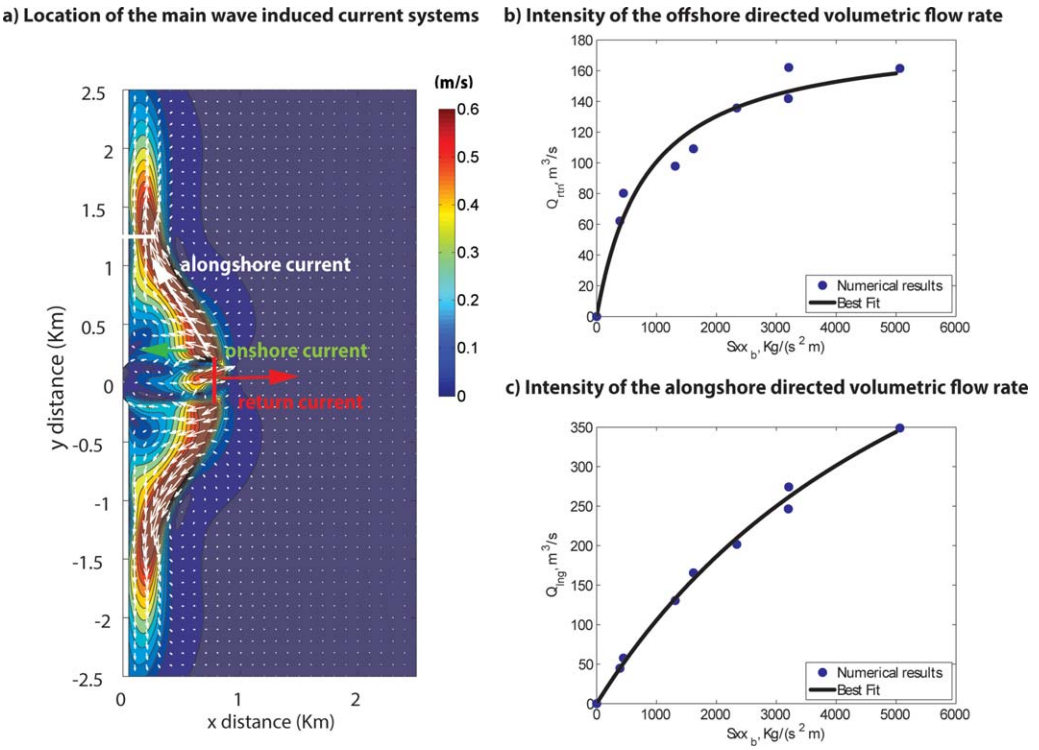

Figure 3. Net volumetric flow rate of the main flows observed in the circulation pattern of the BEACH-CHANNEL-SHOAL configuration. (a) Location of the main circulation patterns due to wave propagation (H_s = 1.5 m, T_p = 10 s), (b) alongshore flow rate (Q_{lng}), and (c) return current flow rate (Q_{rtn}) in function of the offshore wave momentum. The best fits shown in the figure are obtained by considering the function $Q = \frac{aS_{xx,b}}{(b+S_{xx,b})}$, where a and b are fitting coefficients.

shoal the wave setup is smaller (since there is no wave breaking) leading to an alongshore pressure gradient. The oblique incidence of waves with respect to the bathymetry of the shoal and the pressure gradient force an alongshore current (Figure 2h) directed to both sides of the shoal. Over the main channel wave breaking-induced accelerations and the wave setup are smaller due to higher water depths. The alongshore gradient of the wave setup between the shoal and the channel produces a flow convergence toward the channel and consequently a return (offshore-directed) current centered in the main channel. From this point forward this effect will be termed as "return-current" effect.

The cross-shore gradient of the wave setup is higher in the BEACH-CHANNEL-SHOAL than in the BEACH-CHANNEL case. Due to the more intense wave breaking-induced energy dissipation over the ebb shoal the wave setup in the ebb shoal is higher, leading to a more intense return current. Figure 3 depicts the net volumetric flow rate of the main flows observed in the BEACH-CHANNEL-SHOAL configuration (these are indicated in Figure 3a). The volumetric flow rates (Q_{lng} and Q_{rtn}), computed as the integrated flows along the white and red sections shown in Figure 3a, are compared to the cross-shore wave momentum flux before the breaking point (i.e., Sxx_b).

The offshore wave momentum flux before the breaking point (Sxx_b) is the key factor influencing the volumetric flow rate. Both the offshore (Q_{rtn}) (Figure 3b) and the alongshore (Q_{lng}) directed (Figure 3c) flow rates increase with Sxx_b. However, while the alongshore flux shows an increase, the offshore flux saturates for the most energetic wave conditions. The ebb shoal geometry (e.g., the delta shape, extension, and minimum water depths over the shoal) affects the alongshore and cross-shore gradients of the wave momentum flux and therefore are expected to modify the intensity of the observed fluxes.

The vertically averaged momentum balance analysis (not shown) has revealed that with the presence of the ebb shoal, main balance occurs between the wave breaking-induced acceleration which acts in the wave breaking direction (toward the inlet), the bottom friction, the horizontal advection, and the pressure gradient (directed offshore). Maximum horizontal vortex force is observed in the region between the shoal and the channel, where the vorticity is strongest.

4.2. Jet Outflow With No Waves: The Influence of Morphology

For the selected flow rates (Q = 325, 750, 1500, 2250 m^3/s), eddy viscosity (1.0 m^2/s), and bottom friction parameter ($c_f = 0.002$) all the pure jets, except the case with the highest outflow rates in the BEACH-CHANNEL case, were stable and no meanders were observed. c_f is a friction coefficient which depends on the Chezy coefficient (*C*) and on the gravitational acceleration ($c_f = 2g/C^2$). With Q = 1500 and 2250 m^3/s weak meanders were identified in the far zone. Shallow water depths in the BEACH-CHANNEL-SHOAL case in the vicinity of the ebb shoal damped the formation of the meanders.

The value of the stability parameter (S) based on the channel width-to-depth ratio (as defined by *Jirka* [1994]) is 0.075, which is close to the proposed critical jet stability parameter (S_c) values ($0.06 < S_c < 0.6$; e.g., *Jirka* [2001]). The "river mouth" Reynolds number (R_{eB}) as defined by *Canestrelli et al*. [2014] varies from 1.1×10^8 to 3.3×10^8. The stability diagram for shallow water jets presented by *Canestrelli et al*. [2014] classifies the jets with these stability and Reynolds numbers as transition zone jets.

Figure 4 shows the module of the current intensity and the current vectors for each of the inlet configurations and a water discharge of 1500 m^3/s (moderate ebb flow conditions). In the absence of an ebb shoal, the jet centerline velocity decreases exponentially offshore the bar (Figure 4d) with maximum current velocities in the shallowest part of the bar. The momentum balance analysis (not shown here) indicated that offshore the shallowest point of the bar, the pressure gradient term in the cross-shore direction is negligible, and the balance occurs mainly between the onshore-directed bottom friction and the offshore-directed advection terms, similar to the findings of *Hench and Luettich* [2003]. Due to the large bathymetric changes at the edges of the main channel, the lateral mixing in these areas also becomes important. This balance is in agreement with assumptions made by *Ozsoy and Unluata* [1982] who, assuming self-similarity with respect to the jet centerline, derived an analytical solution of the two-dimensional turbulent jet equations for flat and constant sloping beds. They assumed that the jet dynamics were the result of the balance between horizontal advection, bottom friction, and lateral mixing of momentum.

The jet structure in the presence of the ebb shoal clearly shows three distinct regions. The first one corresponds to the area of the ebb shoal, the second one to the abrupt transition between the beach profile and the ebb shoal and the third to the offshore area. Although in all these regions the centerline velocity decays exponentially, the rate of decay varies, because of variations of bed slopes and bottom friction. Overall, the centerline velocity decay is higher in the presence of the ebb shoal, indicating that this morphological element acts to enhance friction by reducing water depth. While without the ebb shoal the jet width is almost constant, the ebb shoal produces a jet spreading similar to the width of the ebb shoal. Only in the third region (offshore of the shoal) the pressure gradient in the cross-shore direction can be neglected. The vertical distribution of the pressure gradient term is uniform. The vertical stress divergence balances advection in this region, similarly to the jet in the absence of a shoal.

When Coriolis acceleration is considered, the Rossby number varies between 1 and 10 (depending on the strength of discharge, indicating a slight to moderate influence of rotation). Figure 4c shows the role of Coriolis force in producing deflection of the jet toward the south. While in the BEACH-CHANNEL case (not shown) the deflection affects the whole jet, in the case of the BEACH-CHANNEL-SHOAL configuration its effect is only noticeable in the third region (offshore the shoal).

4.3. Waves Effects on Currents

In combined jet and wave flows, the flow field and the contribution of wave-current interaction strongly depend on the presence of the ebb shoal and main channel. Without the ebb-shoal, nonbreaking waves (Figure 5b) create an increase of the inlet current intensity of approximately 0.2 m/s, due to the effect of the offshore-directed wave-induced flow. Offshore the inlet region the Lagrangian velocities are slightly reduced because of the onshore-directed Stokes drift. Under breaking wave conditions (Figure 5c) the effect of waves is more dramatic. First, the offshore extension of the jet is greatly reduced primarily because of wave breaking-induced accelerations (see Figure 5d, the increase of the apparent bed roughness due to waves is not considered in these simulations). In this specific case, both depth limitation and opposing currents contribute to the wave breaking. Second, the lateral extent of the jet is increased. At both sides of the channel, wave-induced circulation has an onshore-directed component and a convergence toward the inlet. The third effect of waves is the generation of vorticity at the head the jet. These vortices result from a feedback mechanism between waves and currents, as described in section 5.4.

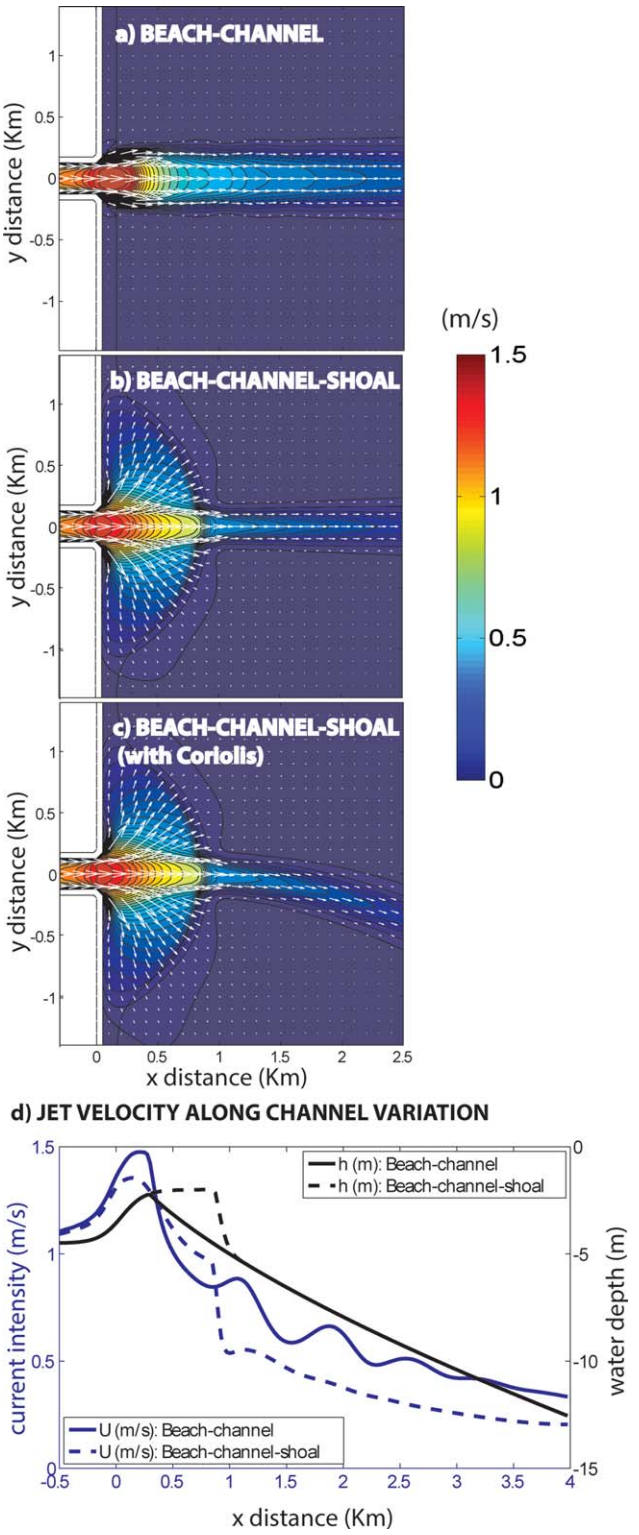

Figure 4. Pure jet intensity spatial distribution, $Q = 1500$ m^3/s. (a) BEACH-CHANNEL case, without Coriolis; (b) BEACH-CHANNEL-SHOAL case, without Coriolis; (c) BEACH-CHANNEL-SHOAL case, with Coriolis; and (d) jet velocity intensity variation in the along channel direction through a section located in the middle of the channel for the BEACH-CHANNEL and BEACH-CHANNEL-SHOAL cases (the case with Coriolis is not shown in this figure).

With the presence of the ebb shoal (Figure 6), breaking waves also reduce the extension of the jet, and significantly modify flows around the inlet. As shown in Figure 3a, the wave-induced circulation is composed of an onshore-directed current over the shoal, an offshore-directed current at the end of the main channel, and the alongshore currents that flow along the edge of the ebb shoal. The strength of this circulation in the presence of a jet flow depends on the relative strength of the jet and wave momentum fluxes. The intensity of wave-induced currents increases as the wave momentum flux increases and the jet momentum flux decreases. In weak jet outflow and strong wave conditions ($Q = 325$ m^3/s and $H_s = 1.5$ m), currents in the shoal are directed onshore and an offshore-directed return current is formed to balance the mass transport toward the shore. As the jet intensity increases ($Q = 750$ m^3/s and $H_s = 1.5$ m), the effect of the jet extends all over the shoal (Figure 6) and the onshore-directed surf zone flow weakens. For the strongest jet flow conditions the onshore-directed flow completely disappears. Thus the flow convergence at the mouth of the main channel and subsequent offshore-directed flow does not occur. In addition, the offshore extent of the jet is reduced by onshore-directed wave breaking-induced acceleration.

Analysis of the terms in the momentum balance (Figure 7) indicates that horizontal advection, bottom friction, and pressure gradient are of comparable strength for the pure jet case. In the presence of waves, the wave breaking-induced acceleration and pressure gradient dominate the balance in the surf zone, with a relatively diminished role of friction and advection. For the combined jet and waves, friction and advection are still important in the outflow jet. In the shallowest part of the ebb shoal (near the offshore edge of the channel) there is

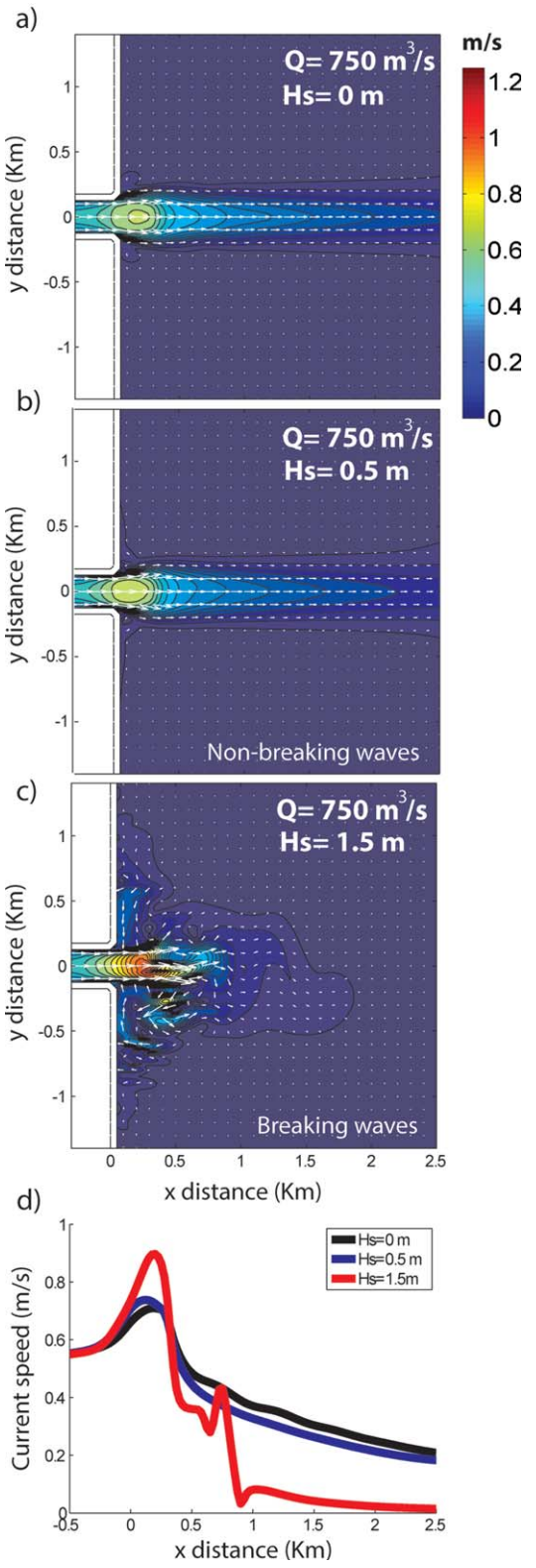

Figure 5. Current intensity (m/s) and current vectors in the BEACH-CHANNEL case for an outflow condition of 750 m^3/s and different significant wave height conditions ($T_p = 10$ s, $\theta = 90°$): (a) $H_s = 0$ m, pure jet flow; (b) $H_s = 0.5$ m; and (c) $H_s = 1.5$ m. (d) The current speed variation along the center of the main channel in function of the significant wave height.

an imbalance between the pressure gradient and the wave breaking-induced accelerations. At these locations, advective acceleration plays a more dominant role in balancing the pressure gradient. Because of the strong opposing currents at the head of the main channel, the wave breaking-induced acceleration term is higher for the combined case than for the pure wave case. Figure 8 shows the variation (along the center of the main channel) of the terms affecting the x component of the depth averaged momentum balance (BEACH-CHANNEL-SHOAL configuration, $Q = 1500$ m^3/s, $H_s = 1.0$ m, and $T_p = 7.5$ s). At the head of the main channel, the wave breaking-induced acceleration acts in the direction opposing to the jet. This is balanced mainly by the pressure gradient term, which is induced by the sharp variation of the wave setup at the edge of the ebb shoal, and the horizontal advection. In the shoaling region, before waves start to break, the wave set down gradient induces a pressure gradient directed in the opposite direction to the jet, but its contribution to the momentum balance is less relevant.

Figure 9a shows the variation of the current intensity at the jet centerline with the distance from the inlet mouth, for BEACH-CHANNEL-SHOAL configuration and for different jet outflow rates and wave conditions. In weak current conditions ($Q <= 750$ m^3/s), waves increase the intensity of the flow at the edge of the shoal (0.9 km) due to the "return-current" effect previously mentioned. In the far field, a reduction of the current intensity is observed as a consequence of the wave breaking acceleration at the head of the main channel. This force affects the outflow rate at the end of the main channel, and therefore the flow intensity in the far field. As the jet flow increases, the effect of the return current system on enhancing the jet also loses relevance. For the strongest outflow conditions waves mainly reduce the offshore extension of the jet at the end of the main channel.

The increase of the offshore H_s (Figure 9b) and T_p (Figure 9c) generate a reduction of the current intensity all along the channel and offshore. However, in the most energetic wave conditions there are significant variations in current speed offshore of the channel.

Figure 10 shows the offshore-directed volumetric flux (q) normalized with the flux corresponding to the pure jet condition (q_0) as

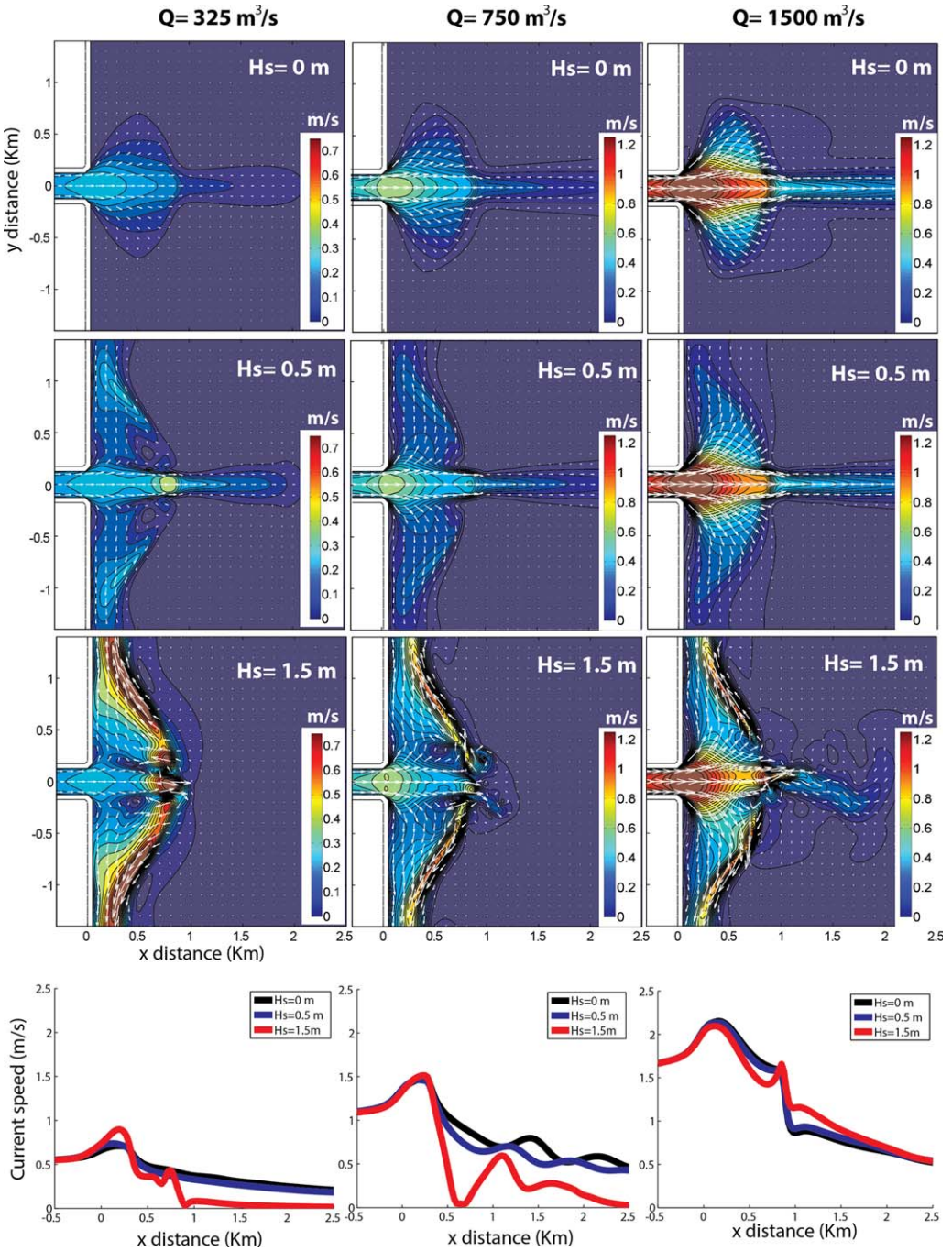

Figure 6. Current intensity (m/s) and current vectors in the BEACH-CHANNEL-SHOAL case for different outflow and significant wave height conditions ($T_p = 10$ s, $\theta = 90°$). Note that the color scale in the first column figures is different. The figures in the last row show the current speed variation along the center of the main channel in function of the significant wave height for the considered outflow conditions. The sections correspond to snapshots after 24 h of simulation.

a function of the wave momentum flux at the breaking point and the jet discharge. The offshore-directed volumetric flux has been computed as the flow integrated along the red section shown in Figure 3a. Due to the reduction of the jet extension, primarily induced by wave breaking, the cross-shore flux between the shoal and the offshore gets reduced trapping the water in the ebb-shoal area and enhancing the alongshore currents. This effect (noticeable in the figure as a reduction of the value of q/q_0) becomes more relevant with increasing wave momentum flux. The opposite occurs as the jet outflow increases. For $Q = 750$ m^3/s (weak jet outflow, indicated in the figure with the blue

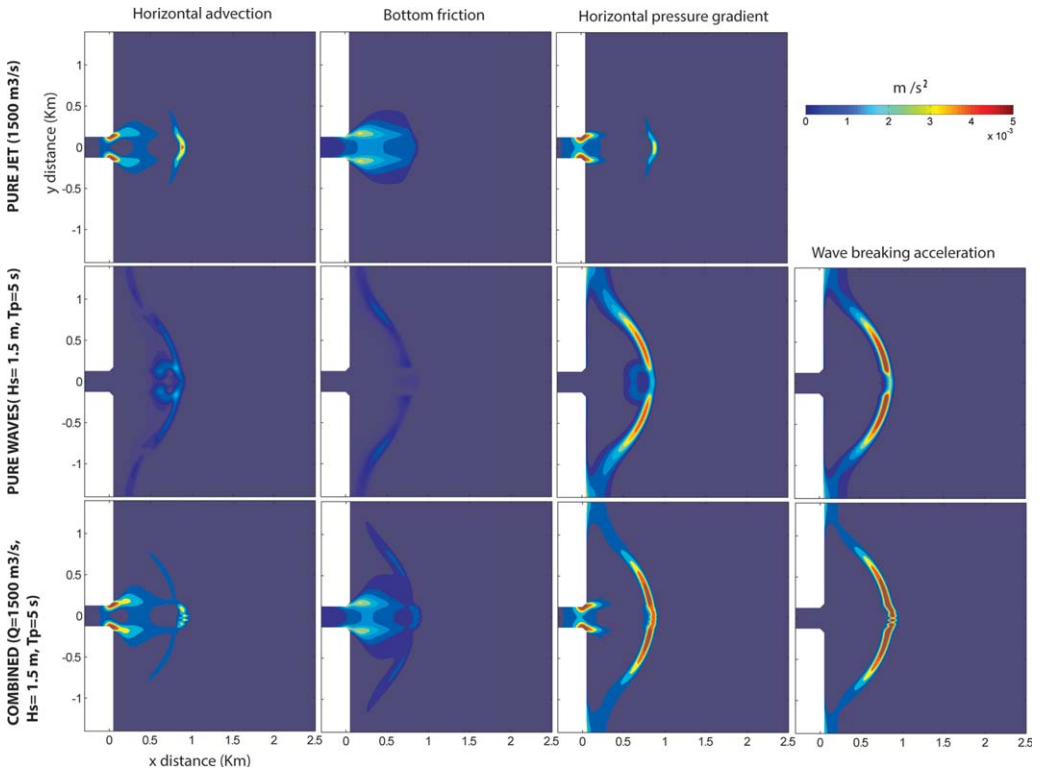

Figure 7. Absolute value of the main terms of the depth averaged momentum balance. Figures in the top represent the main momentum balance terms for a pure jet condition (Q = 1500 m^3/s), those in the middle represent a pure wave case (H_s = 1.5 m, T_p = 5 s, $\theta = 90^\circ$), and those in the bottom a combined jet + wave case (H_s = 1.5 m, T_p = 5 s, $\theta = 90^\circ$, and Q = 1500 m^3/s).

dots) and small values of wave momentum flux, the offshore-directed volumetric flux increases with respect to the pure jet case (q/q_0 is greater than 1). This enhancement results from the wave-induced return-current. For higher wave momentum fluxes and higher jet intensities this effect disappears.

4.4. Currents Effects on Waves

Although the presence of a shoal is the most important factor influencing waves at the inlet, currents also alter wave amplitude and breaking. Intense offshore-directed jets concentrate the wave energy in the channel head by refraction, shoaling and energy advection. If the jet intensity is high enough, the wave length reduction together with the shoaling effect generates a wave that is steep enough to break. Figure 11a shows the variation of the significant wave height along the centerline of the channel when a jet of 2250 m^3/s is present and when no jet is affecting the flow. The increase of the wave height due to the jet is about 0.5 m in all the cases. This enhancement of the wave height at the entrance of the main channel produces an increase of the wave breaking-induced acceleration and results in a greater reduction of the offshore jet extension (Figure 11d).

As the jet intensity increases, the maximum wave height offshore the shoal increases (Figure 11c). An enhancement of the wave peak period also results on an increased wave height amplification in the channel entrance (Figure 11b) which feedbacks to reduce the extension of the jet in the offshore region (Figure 11e). Only when the effects of currents are considered in the wave propagation, the jet offshore the main channels shows undulating patterns due to vorticity variations described in section 5.4.

4.5. Vorticity Changes Due To Wave-Current Interaction

While the vorticity associated with the pure jet field is maximum at the edges of the main channel (Figure 12a), the maximum vorticity for the wave-induced circulation is obtained in the offshore edge of the ebb shoal and especially at the edges of the offshore end of the main channel (Figure12b). The positive and negative vorticity regions observed at the edges of the head of the main channel represent the return-current feeders. When waves interact with the jet (Figure 12c), the vorticity at the edge of the shoal

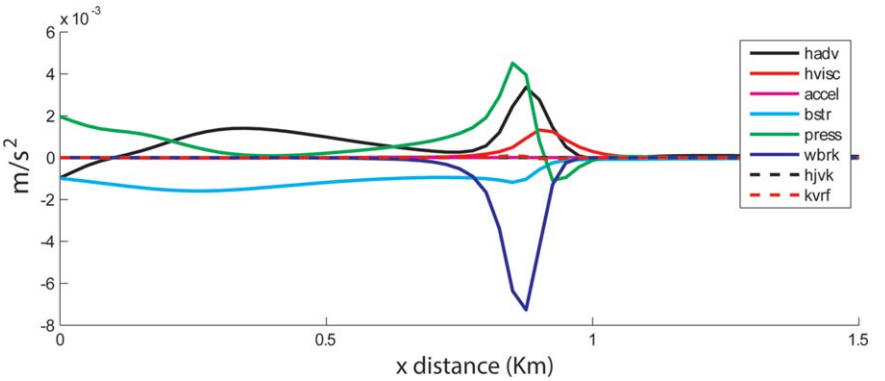

Figure 8. Depth averaged x-momentum balance terms along the center of the main channel in the CHANNEL-SHOAL case (Q = 1500 m^3/s, H_s = 1 m, T_p = 7.5 s). (hadv = horizontal advection; hvisc = horizontal viscosity; accel = local acceleration; bstr = bottom friction; press- = pressure gradient; wbrk = wave breaking-induced acceleration; hjvk = J vortex force; and kvrf = K vortex force terms [see *Kumar et al.*, 2012].)

increases. In the offshore limit of the main channel, at the edges of the channel, the vorticity decreases whereas in the center main channel increases. There is a high vorticity region near the channel end that it is not present when the vorticity of the pure jet and pure cases are linearly added (Figure 12d). The interaction between waves and the jet generates vorticity in the center part of the channel and suppresses the return current feeders.

5. Discussion

In this section, the relevance of bottom friction and eddy viscosity on the observed flows is discussed. Since during the ebb phase the water depths in the inlet are expected to change, we analyze how the depth

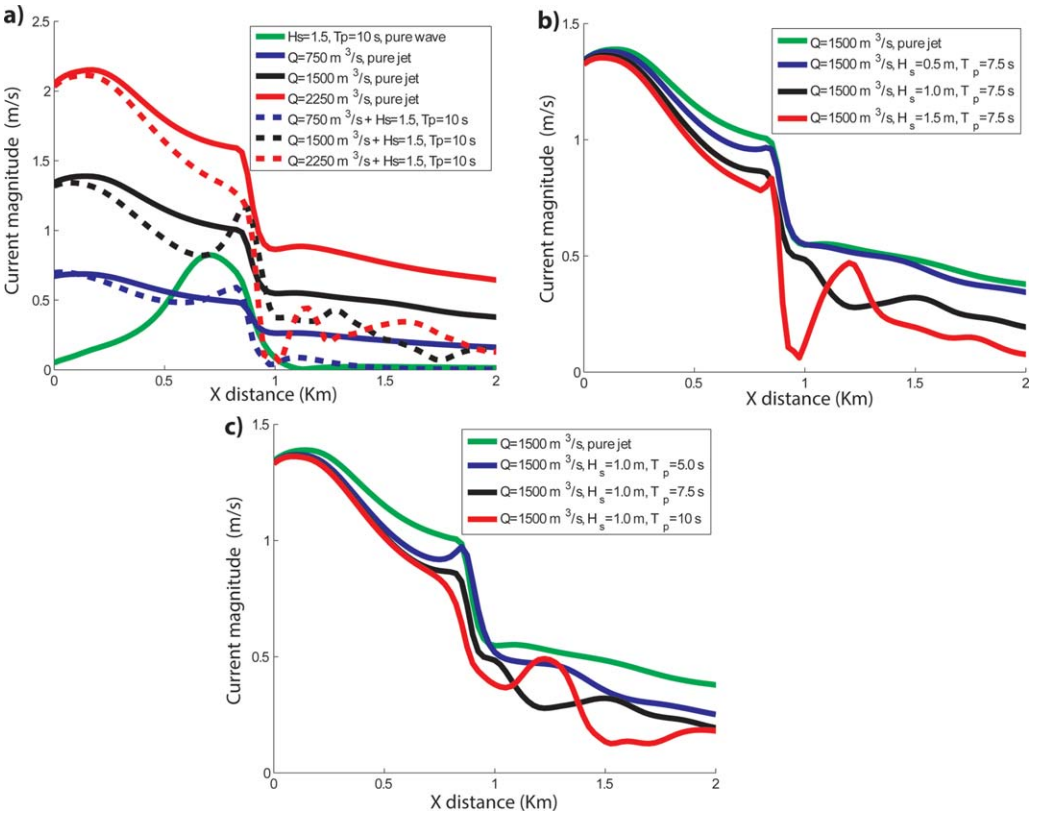

Figure 9. Effect of waves on the jet centerline intensity (a) as a function of the jet intensity, (b) as a function of the significant wave height, and (c) as a function of the peak period. The sections correspond to snapshots after 24 h of simulation.

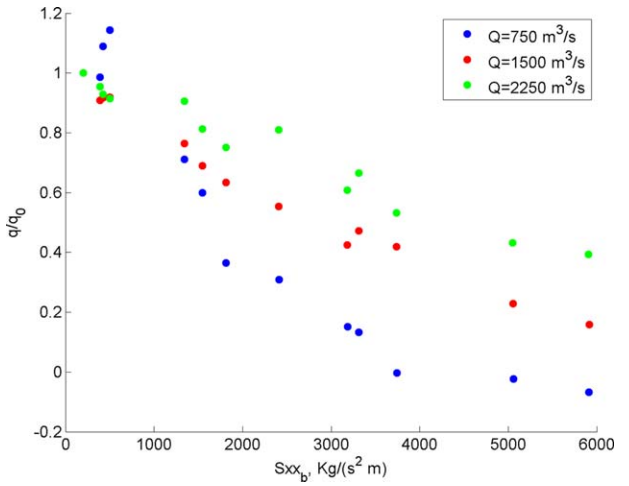

Figure 10. Effect of the wave momentum flux at the breaking point on the relative volumetric flux through the main channel to the offshore. Note that the volume transport (q) has been normalized with the transport corresponding to the pure jet condition (q_0).

variations can affect the aforementioned wave effects on currents. Finally, we discuss how wave-induced effects on currents can be relevant from the sediment transport perspective, morphology, and can also affect the water and tracer exchange mechanisms between the inner estuary and the continental shelf.

5.1. Relevance of Bottom Friction and Eddy Viscosity

As mentioned in the model setup section, all the numerical simulations have been performed assuming a constant bottom roughness and horizontal eddy viscosity values. The results can be sensitive to the values of the eddy viscosity and bottom friction, since they primarily affect the extension and the entrainment of the jet flow. However, although the results could vary quantitatively, the morphological control and the importance of wave-current interaction are expected to be similar. In order to demonstrate this hypothesis, four more runs were performed considering the BEACH-CHANNEL-SHOAL configuration. In the first two runs an enhanced bottom roughness given by the model of *Madsen* [1994] was considered, while in the third and fourth experiments the eddy viscosity was decreased to 0.5 m/s^2. The results are shown in Figure 13. Independently of the eddy viscosity and the bottom roughness values, waves reduce the jet extension and force alongshore directed flows, as described in the former sections. However, the increase of the bottom friction results in a reduction of the magnitude of the observed flows and reduces the intensity of the observed wave-current instabilities, as identified by *Nardin et al.* [2013] and *Canestrelli et al.* [2014] under nonbreaking wave conditions. Reducing the eddy viscosity the vorticity motions as well as the alongshore currents become more intense (Figure 13c).

5.2. Influence of the Water Depths Over the Shoal

In storm conditions, since the jet outflow intensity changes along the ebb period, we would expect to have a variation from a wave-dominated circulation (close to the slack water) to a jet-dominated circulation during the maximum ebb. However, during the ebb not only the intensity of the tidal currents changes but also the water depths. For a progressive tidal wave the velocities and the free surface elevations are in phase whereas in a standing tide there is a 90° phase difference. This phase difference is relevant since it defines the wave breaking-induced acceleration magnitude for a given jet discharge and therefore the relative effect of the wave-induced circulation and jet induced circulation. Figure 14 shows the effect of the water depth on the resultant circulation in the inlet. In this simulation the jet momentum flux was modified for each water depth to maintain the velocity in the inlet equal to 1.0 m/s. The offshore wave characteristics are the same in all cases and the only parameter that changed is the water depth. As the mean water depth decreases over the shoal the alongshore current intensity increases because of the increase of the wave energy dissipation due to the depth-limited breaking (Figures 14a and 14b). However, as the water depth increases the vorticity generation is more intense, mainly because the energy dissipation over the shoal is smaller (Figure 14c).

5.3. Similarities to Rip Current Systems

With the presence of the ebb shoal and a well-developed main channel, the wave-induced circulation is similar to rip current systems, with the effects of wave-current interaction similar to those observed in smaller scale rip currents formed in barred beaches. There are two main differences between the rip current systems identified in the present study and those observed within the surf zone. The first one is the spatial scale. While the rip systems associated with beach bars have scales of hundreds of meters, the rip currents associated with this kind of inlets depend on the main channel width and on the extension of the ebb shoal, which are a

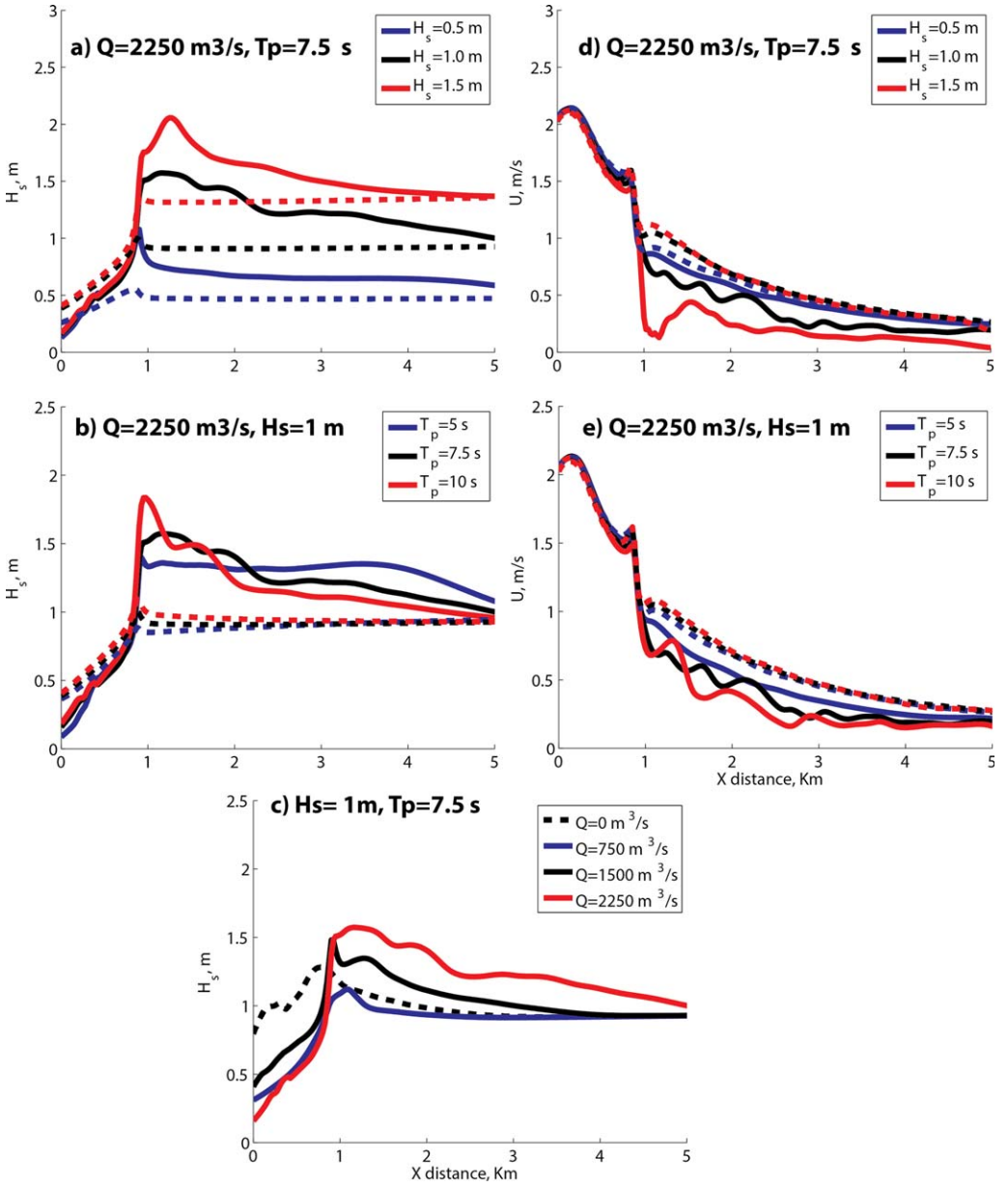

Figure 11. Effect of currents on waves. H_s distribution along the center of the channel for different (a) offshore significant wave heights considering and without considering the effect of currents on waves, (b) offshore wave peak periods considering and without considering the effect of currents on waves, (c) jet outflows. Jet intensity distribution along the center of the channel for different (d) offshore significant wave heights considering and without considering the effect of currents on waves, (e) offshore wave peak periods considering and without considering the effect of currents on waves. Dotted lines in Figures 11a, 11b, 11d, and 11e represent those cases in which currents effect on waves is not considered. The sections correspond to snapshots after 24 h of simulation.

function of the tidal prism in estuarine systems [see *Walton and Adams*, 1976; *O'Brien*, 1969; *Jarrett*, 1976]. The second difference is the location of the feeder flows. In the case of rip currents associated with alongshore variable sand bars observed in the surf zone, the feeder flow is at the shoreward face of the longshore bar [*Yu and Slinn*, 2003]. In the case of the BEACH-CHANNEL-SHOAL configuration, feeder currents have a greater extent and cover the edge between the shoal and the main channel. As a consequence of the small offshore-directed setup gradient over the ebb shoal, no offshore-directed undertow is identified in this region. The water accumulation at the shore is compensated by the offshore-directed and the alongshore currents, manifested in form of offshore and alongshore directed barotropic pressure gradient, respectively. In addition, the nonlinear advective acceleration terms become important near the main channel (not shown here). In a

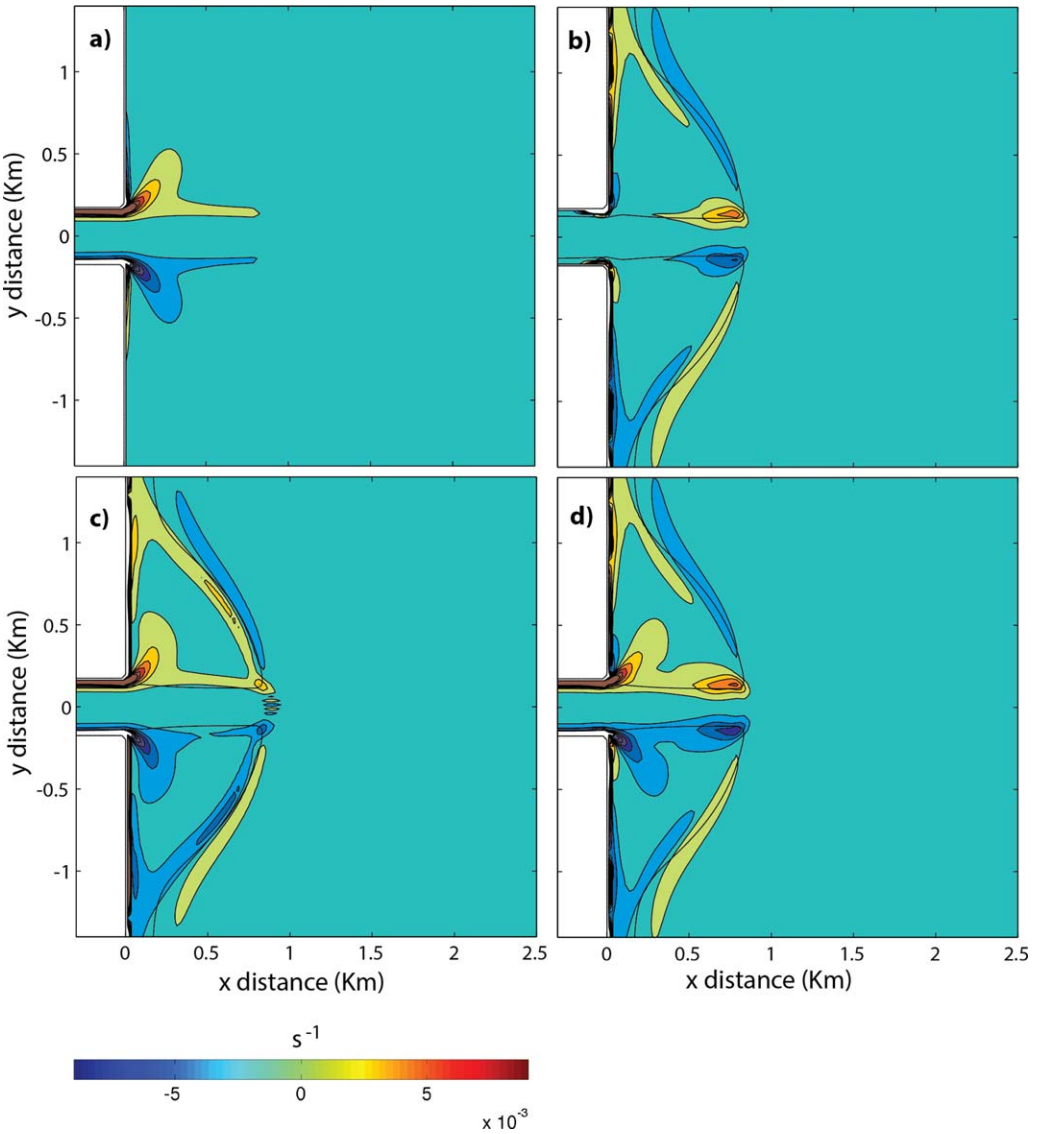

Figure 12. Relative vorticity distribution. (a) Pure jet case, Q = 1500 m^3/s (BEACH-CHANNEL-SHOAL); (b) pure wave case, H_s = 1.5 m T_p = 7.5 s (BEACH-CHANNEL-SHOAL); (c) combined jet-wave case, H_s = 1.5 m T_p = 7.5 s + Q = 1500 m^3/s; and (d) linear addition of pure jet and pure wave vorticities.

strong current regime the feeder currents from the ebb shoal toward the channel are cancelled and strong jet instabilities are observed in high wave and jet outflow conditions.

5.4. Increase of Vorticity and Jet Instability Due To Wave-Current Interaction

The increase of vorticity at the end of the main channel identified in combined jet-wave conditions results from a feedback mechanism between waves and currents. Strong opposing currents produce wave focusing and breaking. Initially, the maximum jet velocity is located in the central part of the channel and is where wave breaking due to currents is highest. As wave breaking increases, it reduces the jet strength in the central part of the channel due to the opposing acting wave breaking-induced accelerations. As a result the jet weakens in the central region (the wave breaking decreases) but becomes more intense at the edges, where wave breaking increases until it is strong enough to reduce the current intensity at the edges and make it stronger again in the center of the channel. These spatial and temporal variations on wave breaking and jet intensity result on the generation of vortexes and enhancement of the jet instability. The vortexes are advected toward the nearshore by the Lagrangian currents (Stokes Drift + Eulerian mean currents) and also to the offshore by a vortex shedding mechanism. Similar jet instabilities have been

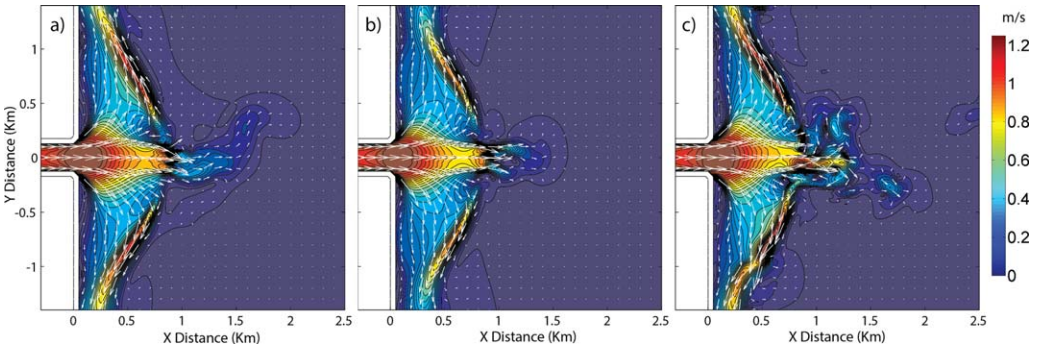

Figure 13. Effect of eddy viscosity and bottom friction on the inlet current system ($H_s = 2$ m, $T_p = 7.5$ s, normal incident waves, $Q = 1500$ m^3/s): (a) eddy viscosity 1 m^2/s and no apparent bed roughness enhancement due to waves, (b) eddy viscosity 1 m^2/s and apparent bed roughness enhancement by *Madsen* [1994], and (c) eddy viscosity 0.5 m^2/s and no apparent bed roughness enhancement due to waves.

previously identified in rip current systems and they are associated with the ejection of vorticity [*Kennedy and Zhang*, 2008]. As explained by *MacMahan et al.* [2006], the rip current shear (approximated by the relation between the rip intensity and the width of the rip channel), determines the potential for the onset of rip current instabilities [*Haller and Dalrymple*, 2001]. In the idealized inlets considered in the present study, jet instabilities are only formed if the effect of currents is included in the wave propagation, and only under high wave and strong current conditions. Once the instabilities are initiated, they affect the wave propagation inducing oscillations on the wave properties near the channel mouth region, reinforcing the instabilities. As a consequence, the resultant hydrodynamic field oscillates over the time and space, producing a statistically stationary but time-dependent solution.

5.5. Similarity to Other Studies

The present study corroborates the findings by *Shi et al.* [2011], who identified large pressure gradient-driven nearshore circulations in the tidal inlet-shoal of San Francisco Bay.

As in the study performed by *Bertin et al.* [2009], we have identified onshore-directed flows in the shoal area and flow convergence toward the inlet mouth due to the effect of waves, when the ebb shoal is present in the inlet morphology. *Bertin et al.* [2009] observed, through numerical simulations, onshore-directed wave-induced flows in Obidos inlet (Portugal) and pointed out the relevance of these flows on contributing to the infilling of the inlet during storm conditions. These flows occur due to an imbalance between the offshore-directed wave setup-induced barotropic pressure gradient and onshore-directed wave breaking-induced acceleration, and could be related with the onshore swash bar migration measured by *Robin et al.* [2009] in a macrotidal inlet located in Normandy (France). *Ranasinghe et al.* [1999] and *Ranasinghe and Pattiaratchi* [2003] proposed that inlet infilling events are caused by small shore normal incident waves, and that larger and steeper waves can keep the inlet open. *Ranasinghe and Pattiaratchi* [2003] assumed that the alongshore and cross-shore currents could be treated separately. We have shown that there is an important

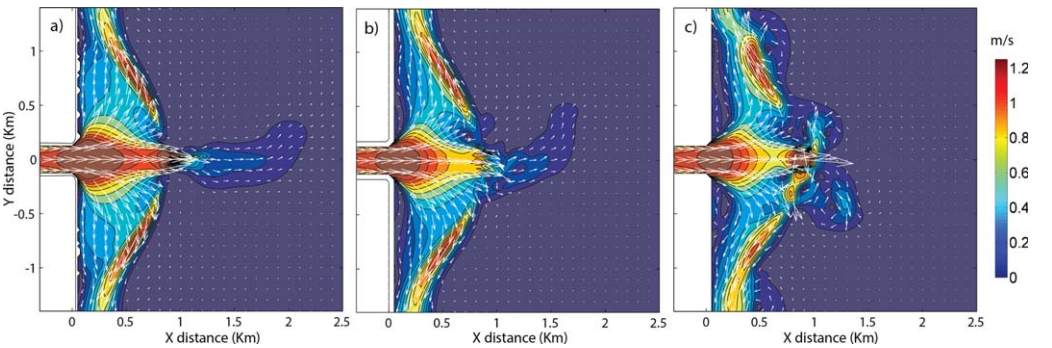

Figure 14. Effect of the water depths over the shoal ($H_s = 2$ m, $T_p = 7.5$ s, normal incident waves, $Q = 1500$ m^3/s): (a) the mean water depth over the shoal is 1.5 m, (b) the mean water depth over the shoal is 2 m, and (c) the mean water depth over the shoal is 2.5 m.

dependency between the alongshore and onshore currents in the inlet area, especially when the ebb shoal and the main channel are present. The onshore-directed flows identified in the present study, and also observed by previous authors [*Bertin et al*., 2009; *Robin et al*., 2009] can be relevant to explain the sediment transport dynamics in tidal inlets, especially in those inlets characterized by pronounced ebb shoal systems.

5.6. Consequences of Wave-Induced Circulation in Tracer Transport and Morphological Evolution of Inlets

The effect of the inlet morphology and wave-current interactions also affect the evolution of other tracers such as pollutants and fecal indicator bacteria, with direct implications on water renewal and water quality problems. Waves can have an important effect during moderate and high wave conditions. Depending on the relative strength of the jet momentum flux and the wave breaking-induced accelerations over the shoal, the wave-induced circulation can significantly modify the circulation patterns in the ebb shoal region, producing a reduction of the jet extension in the offshore area and intensifying the alongshore directed currents in the edge of the ebb shoal. As an example Figure 15 shows the differences on the dye concentration field obtained in the idealized inlet cases. In all these simulations the dye is released constantly and homogeneously along the channel from the beginning of the simulation. Without the effect of the ebb shoal, the dye concentration after 2 h of simulation shows more offshore spreading than in the case with the presence of the ebb shoal. The ebb shoal increases the lateral spreading, and the abrupt water depth changes between the offshore region and the shoal produces a large gradient in the current velocities and therefore in dye concentration. With the presence of the ebb shoal the wave breaking-induced accelerations produce the onshore-directed currents over the ebb shoal and alongshore currents along the edge of this morphological element. Wave-induced circulations can lead to the dye trapping in the ebb shoal region and the subsequent transport to the adjacent beaches through alongshore currents.

It is worth mentioning that the intensity of the wave-induced forces depends on the wave breaking at the edge of the ebb shoal. Wave-dominated inlets exhibit steeper slopes on their seaward margins than tide-dominated inlets [e.g. *Buonaiuto and Kraus*, 2003]. These slopes are in general higher than those observed in beach areas. An increase of the seaward margin of the ebb shoal would result in an increase of the wave breaking-induced acceleration and therefore would enhance the effect of waves in the inlet circulation. In the inlet morphological models proposed by *Hayes* [1980] and *FitzGerald et al*. [2000], the bypassing of sediment occurs through the formation, landward migration, and attachment of large bar complexes to the downdrift shoreline. The development of bar complexes results from stacking and coalescence of swash bars in the delta platform [*FitzGerald et al*., 2000]. In these models is the wave-swash which causes the onshore migration of the "swash bars." The present study has shown that wave breaking-induced accelerations can create strong onshore-directed flows along the ebb shoal platform. The effect of these currents could significantly contribute to the onshore bar migration and therefore affect the bypassing processes in inlets. *Nardin and Fagherazzi* [2012] showed that the wave climate plays an important role in the formation and shape of mouth bars. In their model the surf zone circulation was absent, and therefore their results do not consider the effect of the wave-induced circulations identified in the present work. These could affect the shape of the ebb delta as well as the onshore-directed sediment transport rate. *Mariotti et al*. [2013] and *Canestrelli et al*. [2014] showed that in pure jet conditions, the jet stability can have relevant morphodynamic implications in river mouths. While stable jets tend to form a mouth bar, the decrease of the jet instability favors the formation of subaerial levees and elongated channels. Is therefore possible that the vorticity motions identified for strong wave conditions could impact the inlet morphology and deserves further investigations.

6. Summary and Conclusions

In this study, a coupled three-dimensional, wave-current modeling system (COAWST) has been applied to analyze the hydrodynamic conditions associated with plane jets and wind waves in two different idealized inlet configurations.

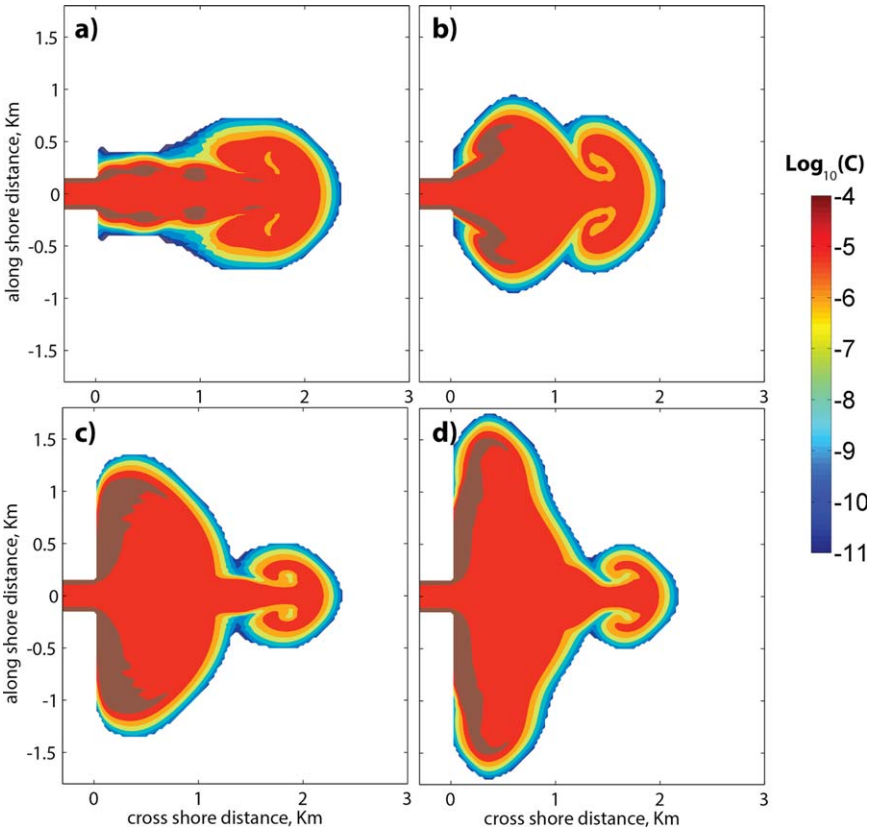

Figure 15. Dye concentration distribution (logarithm of dye concentration) after 2 h of simulation. (a) Pure jet case, Q = 750 m^3/s (BEACH-CHANNEL); (b) pure jet case, Q = 750 m^3/s (BEACH-CHANNEL-SHOAL); (c) combined jet-wave case, H_s = 1 m + Q = 750 m^3/s (BEACH-CHANNEL); and (d) combined jet-wave case, H_s = 1 m + Q = 750 m^3/s (BEACH-CHANNEL-SHOAL).

We have shown that the effects of normal incident waves on jet hydrodynamics are highly dependent on jet outflow rate, offshore wave energy, and inlet morphology. The ebb shoal is a morphological element present in most natural inlet systems and results from the feedbacks between hydrodynamics and sediment transport processes. Due to the reduced water depths, the shoal modifies the wave propagation generating an energy convergence toward the shallowest parts. If the wave energy is high enough it induces wave breaking and maximizes the effect of waves on the resulting flow patterns. During low outflow jet conditions, the resulting hydrodynamics are mainly wave driven and are characterized by an offshore-directed flow at the offshore edge of the main channel, an onshore-directed flow over the ebb shoal, and an alongshore directed flow over the edges of the ebb shoal. As the jet outflow increases the onshore-directed flows are cancelled by the outlet flow. If wave energy is high enough and wave breaking is strong, the wave breaking-induced accelerations reduce the extension of the jet and the flow gets confined to the shoal region. Under strong jet outflow and strong wave conditions vorticity motions are produced in the offshore edge of the main channel. These vortical motions are transported by the mean currents in the alongshore direction and offshore.

For weak jet outflow rates, the jet extension intensifies within the main channel, and this effect gets reinforced with the presence of the ebb shoal. Under breaking wave conditions an onshore-directed flow is observed over the ebb shoal. The wave setup in this region is higher than the setup in the adjacent beaches and in the main channel. As a result an offshore-directed flow is created in the channel and alongshore currents directed from the shoal to the beach. However, as the jet outflow increases, the return current loses its relevance and instead of an increase of the jet extension, a decrease is observed. This is mainly due to the wave breaking-induced accelerations in the channel area and the increase of the apparent bed roughness due to the presence of waves. The ebb shoal, by reducing water depths and offshore wave slopes, acts as a roughness element increasing the lateral

jet spreading and reducing its offshore extension. The presence of the main channel crossing the ebb shoal partially counteracts the effect of the shoal.

This study has shown the complexity of wave-current interaction in inlets, even with a simplified and idealized geometry. The hydrodynamics and the relative importance of wave-current interaction are highly dependent on the presence of channels and ebb shoals, in other words, on the inlet configuration. This analysis provides a starting point for the consideration of the morphodynamic interactions between the flow and bathymetry under varying wave and current forcing conditions.

Acknowledgments

We are grateful to the Career Training Interexchange program that facilitated the training period of Maitane Olabarrieta within the USGS. Maitane Olabarrieta also acknowledges funding from the "Cantabria Campus International Augusto Gonzalez Linares Program." We would also like to thank Giovanni Coco, John C. Warner, and Falk Feddersen for their support with this work and constructive suggestions. We are also grateful to the developers of the COAWST modeling system, SWAN, and ROMS models. WRG was supported by ONR grant N00014-13-1–0368. The authors would also like to thank Sergio Fagherazzi, Xavier Bertin, and the third journal reviewer for their suggestions. The data and numerical results used in this paper will made available upon request to the main author.

References

Bates, C. C. (1953), Rational theory of delta formation, *AAPG Bull.*, *37*(9), 2119–2162.

Bertin, X., A. B. Fortunato, and A. Oliveira (2009), A modeling-based analysis of processes driving wave-dominated inlets, *Cont. Shelf Res.*, *29*, 819–834.

Booij, N., R. C. Ris, and L. H. Holthuijsen (1999), A third-generation wave model for coastal regions, Part I. Model description and validation, *J. Geophys. Res.*, *104*(C4), 7649–7666.

Borichansky, L. S., and V. N. Mikhailov (1966), Interaction of river and sea water in the absence of tides, in *Scientific Problems of the Humid Tropical Zone Deltas and Their Implications*, pp. 175–180, UNESCO.

Bruneau, N., P. Bonneton, B. Castelle, and R. Pedreros (2011), Modeling rip current circulations and vorticity in a high-energy mesotidal-macrotidal environment, *J. Geophys. Res.*, *116*, C07026, doi:10.1029/2010JC006693.

Buonaiuto, F. S., and N. C. Kraus (2003), Limiting slopes and depth at ebb-tidal deltas, *Coastal Eng.*, *48*, 51–65.

Canestrelli, A., W. Nardin, D. Edmonds, S. Fagherazzi, and R. Slingerland (2014), Importance of frictional effects and jet instability on the morphodynamics of river mouth bars and levees, *J. Geophys. Res. Oceans*, *119*, 509–522, doi:10.1002/2013JC009312.

Chapman, D. C. (1985), Numerical treatment of cross-shelf open boundaries in a barotropic coastal ocean model, *J. Phys. Oceanogr.*, *15*, 1060–1075.

Chassignet, E. P., H. G. Arango, D. Dietrich, T. Ezer, M. Ghil, D. B. Haidvogel, C.-C. Ma, A. Mehra, A. M. Paiva, and Z. Sirkes (2000), DAMEE-NAB: The base experiments, *Dyn. Atmos. Oceans*, *32*, 155–183.

Chawla, A., and J. T. Kirby (2002), Monochromatic and random wave breaking at blocking points, *J. Geophys. Res.*, *107*(C7), 3067, doi: 10.1029/2001JC001042.

Davis, R. A., Jr., and P. L. Barnard (2003), Morphodynamics of the barrier-inlet system, west-central Florida, *Mar. Geol.*, *200*(1–4), 77–101, doi: 10.1016/S0025-3227(03)00178-6.

Dean, R. G. (1977), Equilibrium beach profiles: U.S. Atlantic and Gulf coasts, *Ocean Eng. Rep. No. 12*, Dep. of Civil Eng., Univ. of Delaware, Newark, Del.

Delpey, M. T., F. Ardhuin, P. Otheguy, and A. Jouon (2013), Effects of waves on coastal water dispersion in a small estuarine bay, *J. Geophys. Res. Oceans*, *119*, 70–86, doi:10.1002/2013JC009466.

Dodet, G., X. Bertin, N. Bruneau, A. B. Fortunato, A. Nahon, and A. Rolan (2013), Wave–current interactions in a wave-dominated tidal inlet, *J. Geophys. Res. Oceans*, *118*, 1587–1605, doi:10.1002/jgrc.20146.

Eldeberky, Y., and J. A. Battjes (1996), Spectral modelling of wave breaking: Application to Boussinesq equations, *J. Geophys. Res.*, *101*(C1), 1253–1264.

FitzGerald, D. M., N. C. Kraus, and E. B. Hands (2000), Natural mechanisms of sediment bypassing at tidal inlets, *Coastal Eng. Tech. Note, US Army Corps of Eng. ERDC/CHL CETN-IV-30*, U.S. Army Eng. Res. and Dev. Cent., Vicksburg, Miss.

Haas, K. A., I. A. Svendsen, M. C. Haller, and Q. Zhao (2003), Quasi-three-dimensional modeling of rip current systems, *J. Geophys. Res.*, *108*(C7), 3217, doi:10.1029/2002JC001355.

Haidvogel, D. B., H. G. Arango, K. Hedstrom, A. Beckmann, P. Malanotte-Rizzoli, and A. F. Shchepetkin (2000), Model evaluation experiments in the North Atlantic Basin: Simulations in nonlinear terrain-following, *Dyn. Atmos. Oceans*, *32*, 239–281.

Haidvogel, D. B., et al. (2008), Regional ocean forecasting in terrain-following coordinates: Model formulation and skill assessment, *J. Comput. Phys.*, *227*(7), 3595–3624.

Haller, M. C., and R. A. Dalrymple (2001), Rip currents instabilities, *J. Fluid Mech.*, *433*, 161–192.

Hayes, M. O. (1979), Barrier island morphology as a function of tidal and wave regime, in *Barrier Islands, From the Gulf of St Laurence to the Gulf of Mexico*, edited by S. P. Leatherman, pp. 1–28, Academic, N. Y.

Hayes, M. O. (1980), General morphology and sediment patterns in tidal inlets, *Sediment. Geol.*, *26*, 139–156.

Hench, J. L., and A. Luettich Jr. (2003), Transient tidal circulation and momentum balances at a shallow inlet, *J. Phys. Oceanogr.*, *33*, 913–932.

Ismail, N. M. (1980), Wave-current interaction, *Tech. Rep. HEL 27-7*, Hydraul. & Coastal Eng. Div., Univ. of Calif., Berkeley, Calif.

Ismail, N. M., and R. L. Wiegel (1983), Effect of opposing waves on momentum jets spreading, *J. Waterway Port Coastal Ocean Div.*, *109*, 465–483.

Jarrett, J. T. (1976), Tidal Prism-Inlet area relationships, *GITI Rep. 3*, U.S. Army Corps of Eng., Waterw. Exp. Stn., Vicksburg, Miss.

Jirka, G. H. (1994), Shallow jets, in *Recent Research Advances in the Fluid Mechanics of Turbulent Jets and Plumes*, edited by P. A. Davies and M. J. V. Neves, pp. 155–175, Kluwer Academic Publishers.

Jirka, G. H. (2001), Large scale flow structures and mixing processes in shallow flows, *J. Hydraul. Res.*, *39*(6), 567–573.

Joshi, P. B. (1982), Hydromechanics of tidal jets, *J. Waterw. Port Coastal Ocean Div.*, *108*(3), 239–253.

Kang, K., and D. Di Iorio (2006), Depth-and current-induced effects on wave propagation into the Altamaha River Estuary, Georgia, *Estuarine Coastal Shelf Sci.*, *66*, 395–408.

Kennedy, A. B., and Y. Zhang (2008), The stability of wave-driven rip current circulation, *J. Geophys. Res.*, *113*, C03031, doi:10.1029/2006JC003814.

Kirby, J. T., and T.-M. Chen (1989), Surface waves on vertically sheared flows: Approximate dispersion relations, *J. Geophys. Res.*, *94*, 1013–1027.

Komen, G. J., S. Hasselmann, and K. Hasselmann (1984), On the existence of a fully developed wind-sea spectrum, *J. Phys. Oceanogr.*, *14*, 1271–1285.

Kumar, N., G. Voulgaris, J. C. Warner, and M. Olabarrieta (2012), Implementation of the vortex force formalism in the coupled ocean-atmosphere-wave-sediment transport (COAWST) modeling system for inner shelf and surf zone applications, *Ocean Modell.*, *47*, 65–95, doi:10.1016/j.ocemod.2012.01.003.

Leonardi, N., A. Canestrelli, T. Sun, and S. Fagherazzi (2013), Effect of tides on mouth bar morphology and hydrodynamics, *J. Geophys. Res. Oceans*, *118*, 4169–4183, doi:10.1002/jgrc.20302.

MacMahan, J. H., E. B. Thornton, and A. J. H. M. Reniers (2006), Rip current review, *Coastal Eng.*, *53*, 191–208, doi:10.1016/j.coastaleng.2005.10.009.

Madsen, O. S. (1994), Spectral wave-current bottom boundary layer flows, in *Coastal Engineering '94, Proceedings of the 24th International Conference*, pp. 384–398, Coastal Eng. Res. Counc./ASCE, Kobe, Japan.

Madsen, P. A., M. Rugbjerg, and I. R. Warren (1988), Subgrid modelling in depth integrated flows, paper presented at Proceedings of the International Twenty-First Coastal Engineering Conference, Malaga, Spain.

Mariotti, G., F. Falcini, N. Geleynse, M. Guala, T. Sun, and S. Fagherazzi (2013), Sediment eddy diffusivity in meandering turbulent jets: Implications for levee formation at river mouths, *J. Geophys. Res. Earth Surf.*, *118*, 1908–1920, doi:10.1002/jgrf.20134.

Masselink, G., and M. G. Hughes (2003), *Introduction to Coastal Processes and Geomorphology*, 354 pp., Edward Arnold, London, U. K.

McWilliams, J. C., J. M. Restrepo, and E. M. Lane (2004), An asymptotic theory for interaction of waves and currents in coastal waters, *J. Fluid Mech.*, *511*, 135–178.

Nahon, A., X. Bertin, A. B. Fortunato, and A. Oliveira (2012), A modeling-based assessment of tidal inlet classification, *Mar. Geol.*, *291–294*, 1–11.

Nardin, W., and S. Fagherazzi (2012), The effect of wind waves on the development of river mouth bars, *Geophys. Res. Lett.*, *39*, L12607, doi:10.1029/2012GL051788.

Nardin, W., G. Mariotti, D. A. Edmonds, R. Guercio, and S. Fagherazzi (2013), Growth of river mouth bars in sheltered bays in the presence of frontal waves, *J. Geophys. Res. Earth Surf.*, *118*, 872–886, doi:10.1002/jgrf.20057.

O'Brien, M. P. (1969), Equilibrium flow areas of inlets and sandy coasts, *J. Waterw. Harbor Coastal Eng. Div.*, *95*, 43–52.

Olabarrieta, M., J. C. Warner, and N. Kumar (2011), Wave-current interaction in Willapa Bay, *J. Geophys. Res.*, *116*, C12014, doi:10.1029/2011JC007387.

Ozsoy, E. (1977), Flow and mass transport in the vicinity of tidal inlets, *Tech. Rep. TR-036*, University of Florida, Coastal and Oceanogr. Eng. Lab.

Ozsoy, E., and U. Unluata (1982), Ebb-tidal flow characteristics near inlets, *Estuarine Coastal Shelf Sci.*, *14*(3), 251–263.

Ranasinghe, R., and C. Pattiaratchi (2003), The seasonal closure of tidal inlets: Causes and effects, *Coastal Eng. J.*, *45*(4), 601–627.

Ranasinghe, R., C. Pattiaratchi, and G. Masselink (1999), The seasonal closure of tidal inlets: Wilson inlet, a case study, *Coastal Eng.*, *37*, 37–56.

Ris, R. C., and L. H. Holthuijsen (1996), Spectral modelling of current wave-blocking, in *Proc. 25th Int. Conf. on Coastal Eng.*, ASCE, pp. 1247–1254.

Robin, N., F. Levoy, and O. Monfort (2009), Short term morphodynamics of an intertidal bar on megatidal ebb delta, *Mar. Geol.*, *260*, 102–120.

Shchepetkin, A. F., and J. C. McWilliams (2005), The regional ocean modeling system (ROMS): A split-explicit, free-surface, topography-following-coordinates ocean model, *Ocean Modell.*, *9*, 347–404.

Shi, F., D. M. Hanes, J. T. Kirby, L. Erikson, P. Barnard, and J. Eshleman (2011), Pressure-gradient-driven nearshore circulation on a beach influenced by a large inlet-tidal shoal system, *J. Geophys. Res.*, *116*, C04020, doi:10.1029/2010JC006788.

Smith, S. J., and J. M. Smith (2001), Numerical modeling of waves at Ponce de Leon Inlet, *J. Waterw. Port Coastal Ocean Eng.*, *127*, 176–184.

Uchiyama, Y., J. C. McWilliams, and A. F. Shchepetkin (2010), Wave-current interaction in an oceanic circulation model with a vortex force formalism: Application to the surf zone, *Ocean Modell.*, *34*(1–2), 16–35.

van der Westhuysen, A. J. (2012), Spectral modeling of wave dissipation on negative current gradients, *Coastal Eng.*, *68*, 17–30, doi:10.1016/j.coastaleng.2012.05.001.

Walton, T. L., and W. D. Adams (1976), Capacity of inlet outer bars to store sand, in *Proceedings of the 15th International Coastal Engineering Conference*, pp. 1919–1937, ASCE, N. Y.

Wargula, A., B. Raubenheimer, and S. Elgar (2014), Wave-driven along-channel subtidal flows in a well-mixed ocean inlet, *J. Geophys. Res. Oceans*, *119*, 2987–3001, doi:10.1002/2014JC009839.

Warner, J. C., B. Armstrong, R. He, and J. Zambon (2010), Development of a coupled ocean-atmosphere-wave-sediment transport (COAWST) modeling system, *Ocean Modell.*, *35*, 230–244.

Weir, B., Y. Uchiyama, E. M. Lane, J. M. Restrepo, and J. C. McWilliams (2011), A vortex force analysis of the interaction of rip currents and surface gravity waves, *J. Geophys. Res.*, *116*, C05001, doi:10.1029/2010JC006232.

Wright, L. D. (1977), Sediment transport and deposition at river mouths: A synthesis, *Geol. Soc. Am. Bull.*, *88*, 857–868.

Wright, L. D., and J. M. Coleman (1974), Mississippi river mouth processes—Effluent dynamics and morphologic development, *J. Geol.*, *82*(6), 751–778.

Yu, J., and D. N. Slinn (2003), Effects of wave-current interaction on rip currents, *J. Geophys. Res.*, *108*(C3), 3088, doi:10.1029/2001JC001105.